High-Spin Molecules: Hexanuclear Mn^{III} Clusters with $[Mn_6O_4X_4]^{6+}$ ($X = Cl^-$, Br^-) Face-Capped Octahedral Cores and $S = 12$ Ground States

Guillem Aromí,[1a] Michael J. Knapp,[1b] Juan-Pablo Claude,[1a,c] John C. Huffman,[1a] David N. Hendrickson,*[,1b] and George Christou*[,1a]

Contribution from the Department of Chemistry and Molecular Structure Center, Indiana University, Bloomington, Indiana 47405-4001, and Department of Chemistry-0358, University of California at San Diego, La Jolla, California 93093-0358

Received September 28, 1998

Abstract: Reaction of R_2dbmH (R = H, Me, Et; dbmH is dibenzoylmethane) with $MnCl_3$ (generated in situ from $MnCl_2$ and MnO_4^-) in MeCN yields the five-coordinate, square-pyramidal complexes $[MnCl(R_2dbm)_2]$ (R = H, **1**; Me, **4**; Et, **7**). The same reaction with $MnBr_2$ yields $[MnBr(R_2dbm)_2]$ (R = H, **2**; Me, **5**; Et, **8**). Slow hydrolysis of **4** or **7** in CH_2Cl_2/MeCN over two weeks gives $[Mn_6O_4Cl_4(R_2dbm)_6]$ (R = Me, **9**; Et, **11**); the crystal structure of **9** reveals a novel $[Mn_6(\mu_3\text{-}O)_4(\mu_3\text{-}Cl)_4]^{6+}$ core comprising an Mn_6^{III} octahedron whose faces are capped by O^{2-} or Cl^- ions. Similar slow hydrolysis of **5** or **8** gives $[Mn_6O_4Br_4(R_2dbm)_6]$ (R = Me, **10**; Et, **12**); the crystal structure of **10** is identical with that of **9** except for the Br^--for-Cl^- substitution. The ^1H NMR spectra of **1**−**12** in $CDCl_3$ show paramagnetically shifted and broadened R_2dbm resonances. The spectra are as expected for retention of the solid-state structures, the Mn_6 complexes exhibiting effective T_d solution symmetry with no evidence of fragmentation to $[MnX(R_2dbm)]$, $[Mn(R_2dbm)_3]$, or any other species. The effective magnetic moment (μ_{eff}) per Mn_6 for **9**/**12** slowly increases from 16.01/16.73 μ_B at 320/300 K to a maximum of 24.37/24.60 μ_B at 30.1/40.0 K, and then decreases to 13.69/13.86 μ_B at 2.00 K. Fitting of the data to the theoretical equation derived for a Mn_6^{III} octahedron gives (for **9**/**12**) $J_{cis} = 8.6/8.5$ cm^{-1} and $g = 1.97/1.98$ with J_{trans} and TIP held fixed at 0 cm^{-1} and 1200 × 10^{-6} cm^3 mol^{-1}, respectively. These values indicate a $S = 12$ ground state. Fitting of magnetization vs field data collected in the 2.00−15.0 K and 0.500−50.0 kG ranges confirmed $S = 12$ ground states with $D \approx 0$ cm^{-1}.

Introduction

The study of molecules possessing unusually large spin (S) values in their ground state is an area of intense current research.[2−5] These efforts are driven by a number of considerations, including the desire to elucidate the various factors responsible for yielding high-spin molecules. These include the topological arrangement of the paramagnetic ions, the nature (ferromagnetic or antiferromagnetic) of the inter-ion exchange interactions, and the presence of spin frustration effects from the presence of competing interactions of comparable magnitude. In addition, it has recently become apparent that a relatively large ground-state S value is one of the necessary requirements for molecules to be able to exhibit the new phenomenon of single-molecule magnetism.[6−12] Another requirement is a significant magnetoanisotropy as reflected in the zero-field splitting (ZFS) parameter D, which needs also to be negative.

(1) (a) Indiana University. (b) University of California. (c) Present address: Department of Chemistry, University of Alabama at Birmingham, Birmingham, AL 35249.

(2) (a) Eppley, H. J.; Tsai, H.-L.; de Vries, N.; Folting, K.; Christou, G.; Hendrickson, D. N. *J. Am. Chem. Soc.* **1995**, *117*, 301. (b) Tsai, H.-L.; Wang, S.; Folting, K.; Streib, W. E.; Hendrickson, D. N.; Christou, G. *J. Am. Chem. Soc.* **1995**, *117*, 2503. (c) Eppley, H. J.; Wang, S.; Tsai, H.-L.; Aubin, S. M.; Folting, K.; Streib, W. E.; Hendrickson, D. N.; Christou, G. *Mol. Cryst. Liq. Cryst.* **1995**, *274*, 159.

(3) Powell, A. K.; Heath, S. L.; Gatteschi, D.; Pardi, L.; Sessoli, R.; Spina, G.; Del Giallo, F.; Pieralli, F. *J. Am. Chem. Soc.* **1995**, *117*, 2491.

(4) (a) Sculiller, A.; Mallah, T.; Verdaguer, M.; Nivorozkhin, A.; Tholence, J.-L.; Veillet, P. *New J. Chem.* **1996**, *20*, 1. (b) Delfs, C. D.; Gatteschi, D.; Pardi, L.; Sessoli, R.; Wieghardt, K.; Hanke, D. *Inorg. Chem.* **1993**, *32*, 3099. (c) Caneschi, A.; Gatteschi, D.; Laugier, J.; Rey, P.; Sessoli, R.; Zanchini, C. *J. Am. Chem. Soc.* **1988**, *110*, 2795. (d) Goldberg, D. P.; Caneschi, A.; Delfs, C. D.; Sessoli, R.; Lippard, S. J. *J. Am. Chem. Soc.* **1995**, *117*, 5789. (e) Blake, A. J.; Grant, C. M.; Parsons, S.; Rawson, J. M.; Winpenny, R. E. P. *J. Chem. Soc., Chem. Commun.* **1994**, 2363. (f) Sun, Z.; Gantzel, P. K.; Hendrickson, D. N. **1996**, *35*, 6640. (g) Benelli, C.; Parsons, S.; Solan, G. A.; Winpenny, R. E. P. *Angew. Chem., Int. Ed. Engl.* **1996**, *35*, 1825. (h) Abbati, G. L.; Cornia, A.; Fabretti, A. C.; Caneschi, A.; Gatteschi, D. *Inorg. Chem.* **1998**, *37*, 1430.

(5) (a) Bolcar, M. A.; Aubin, S. M. J.; Folting, K.; Hendrickson, D. N.; Christou, G. *Chem. Commun.* **1997**, 1485. (b) Tsai, H.-L.; Wang, S.; Folting, K.; Streib, W. E.; Hendrickson, D. N.; Christou, G. *J. Am. Chem. Soc.* **1995**, *117*, 2503. (c) Christou, G. In *Magnetism: A Supramolecular Function*; Kahn, O., Ed.; NATO ASI Series; Kluwer: Dordrecht, 1996.

(6) (a) Sessoli, R.; Tsai, H.-L.; Schake, A. R.; Wang, S.; Vincent, J. B.; Folting, K.; Gatteschi, D.; Christou, G.; Hendrickson, D. N. *J. Am. Chem. Soc.* **1993**, *115*, 1804. (b) Sessoli, R.; Gatteschi, D.; Caneschi, A.; Novak, M. A. *Nature* **1993**, *365*, 141.

(7) (a) Aromí, G.; Aubin, S. M. J.; Bolcar, M. A.; Christou, G.; Eppley, H. J.; Folting, K.; Hendrickson, D. N.; Huffman, J. C.; Squire, R. C.; Tsai, H.-L.; Wang, S.; Wemple, M. W. *Polyhedron* **1998**, *17*, 3005. (b) Tsai, H.-L.; Eppley, H. J.; De Vries, N.; Folting, K.; Christou, G.; Hendrickson, D. N. *Mol. Cryst. Liq. Cryst.* **1995**, *274*, 167.

(8) (a) Aubin, S. M. J.; Wemple, M. W.; Adams, D. M.; Tsai, H.-L.; Christou, G.; Hendrickson, D. N. *J. Am. Chem. Soc.* **1996**, *118*, 7746. (b) Aubin, S. M. J.; Dilley, N. R.; Wemple, M. W.; Maple, M. B.; Christou, G.; Hendrickson, D. N. *J. Am. Chem. Soc.* **1998**, *120*, 839.

(9) (a) Friedman, J. R.; Sarachik, M. P.; Tejada, J.; Maciejewski, J.; Ziolo, R. *J. Appl. Phys.* **1996**, *79*, 6031. (b) Friedman, J. R.; Sarachik, M. P.; Tejada, J.; Ziolo, R. *Phys. Rev. Lett.* **1996**, *76*, 3830.

(10) (a) Tejeda, J.; Ziolo, R. F.; Zhang, X. X. *Chem. Mater.* **1996**, *8*, 1784. (b) Hernandez, J. M.; Zhang, X. X.; Luis, F.; Bartolomé, J.; Tejada, J.; Ziolo, R. *Europhys. Lett.* **1996**, *35*, 301.

10.1021/ja983446c CCC: $18.00
Published on Web 05/27/1999

The development of synthetic procedures to new examples of high-spin molecules is thus of continuing interest.

One area in which high-spin molecules are encountered on a relatively frequent basis is manganese cluster chemistry.[4,5,7] Spin values of $S \leq 12$ have been observed; for calibration, the largest S value observed to date in a molecular species is $S \approx {}^{33}/_{2}$ in a cocrystallized mixture of Fe_{17} and Fe_{19} clusters.[3] We and others have reported several Mn_x clusters with S values ≥ 4,[4,5,7,8,11] and some of these have also proven to be single-molecule magnets. In this paper, we describe two new Mn_6 clusters of formula $[Mn_6O_4X_4(R_2dbm)_6]$ ($X = Cl^-$, Br^-). Not only do they possess very aesthetically pleasing structures comprising the initial examples of the $M_6A_4B_4$ near-tetrahedral core, but they have been found to possess $S = 12$ ground states. Portions of this work have been previously communicated.[13]

Experimental Section

All manipulations were performed under aerobic conditions using materials as received, except where indicated otherwise. $NBu^n_4MnO_4$ was prepared as described elsewhere.[14] dbmH = dibenzoylmethane = 1,3-diphenyl-1,3-propanedione; Me_2dbmH = 4,4′-dimethyldibenzoylmethane; Et_2dbmH = 4,4′-diethyldibenzoylmethane.

$MnCl(dbm)_2$ (1). A stirred solution of $MnCl_2 \cdot 4H_2O$ (0.11 g, 0.56 mmol) in MeOH (3 mL) was treated with a purple solution of $NBu^n_4MnO_4$ (51 mg, 0.14 mmol) in MeCN (6 mL), and to the resulting red-brown solution was immediately added solid dbmH (0.31 g, 1.4 mmol). The mixture was stirred for about 45 min, and the solvents were evaporated to dryness. The residue was washed with Et_2O, and the remaining solid was redissolved in CH_2Cl_2. A small amount of a white powder was removed by filtration, and the solvent was removed to dryness. The solid was washed with Et_2O and dried in vacuo. The yield was 61% based on Mn. Anal. Calcd (Found) for **1**·$0.08CH_2Cl_2$: C, 66.45 (66.43); H, 4.11 (4.22); N, 0.00 (0.00). Crystals suitable for X-ray crystallography were obtained from layering a solution of **1** (25 mg) in CH_2Cl_2 (5 mL) with Et_2O.

$MnBr(dbm)_2$ (2). Solid $MnBr_2 \cdot 4H_2O$ (0.17 g, 0.56 mmol) was dissolved in a stirred yellow solution of dbmH (0.31 g, 1.4 mmol) in MeCN (20 mL), and the resulting solution was treated with a purple solution of $NBu^n_4MnO_4$ (51 mg, 0.14 mmol) in MeCN (10 mL). The mixture was stirred for 2 h, and the brown precipitate was collected by filtration, washed with Et_2O, and dried in vacuo. The yield was 38% based on Mn. Anal. Calcd (Found) for **2**·0.1MeCN: C, 61.96 (61.66); H, 3.84 (3.83); N, 0.24 (0.20).

$Mn(dbm)_3$ (3). To a stirred light pink solution of $Mn(O_2CMe)_2 \cdot 4H_2O$ (55 mg, 0.22 mmol) in MeOH (10 mL) was added a purple solution of $NBu^n_4MnO_4$ (20 mg, 0.056 mmol) in MeOH (5 mL) to give a red-brown solution. This was treated with a solution of dbmH (0.19 g, 0.84 mmol) in MeCN (20 mL), and a brown microcrystalline solid started to precipitate within minutes. After 1 h, the solid was collected by filtration, washed with Et_2O, and dried in vacuo. The yield was 84% based on Mn. Anal. Calcd (Found) for **3**: C, 74.58 (74.40); H, 4.59 (4.69); N, 0.00 (0.00).

$MnCl(Me_2dbm)_2$ (4). To a stirred solution of $MnCl_2 \cdot 4H_2O$ (0.11 g, 0.56 mmol) in MeOH (3 mL) was added a purple solution of $NBu^n_4MnO_4$ (51 mg, 0.14 mmol) in MeCN (6 mL). To the resulting red-brown solution was immediately added a solution of Me_2dbmH (0.35 g, 1.4 mmol) in MeCN (11 mL) which had been warmed slightly to completely dissolve the solid. The mixture was stirred for a few minutes, and the resulting brown microcrystalline solid was collected by filtration, washed with Et_2O, and dried in vacuo. The yield was 47% based on Mn. Crystals suitable for X-ray crystallography were obtained from a layering of a solution of **4** (40 mg) in CH_2Cl_2 (4 mL) with equivolume Et_2O. Anal. Calcd (Found) for **4**·$0.2CH_2Cl_2$: C, 67.34 (67.25); H, 5.02 (5.06); N, 0.00 (0.00).

$MnBr(Me_2dbm)_2$ (5). Solid $MnBr_2 \cdot 4H_2O$ (0.16 g, 0.56 mmol) was dissolved with stirring in a yellow solution of Me_2dbmH (0.35 g, 1.4 mmol) in MeCN (11 mL), which had been slightly warmed to completely dissolve the solid. The solution was then treated with a purple solution of $NBu^n_4MnO_4$ (51 mg, 0.14 mmol) in MeCN (6 mL). After a few minutes, the microcrystalline solid that formed was collected by filtration and washed with Et_2O. The solid was slurried for a few minutes in a 1/1 mixture of $MeCN/CH_2Cl_2$ (10 mL), refiltered, washed with Et_2O, and dried in vacuo. The yield was 25% based on Mn. Anal. Calcd (Found) for **5**·0.1MeCN·$0.55CH_2Cl_2$; C, 60.64 (60.59); H, 4.60 (4.27); N, 0.20 (0.22).

$Mn(Me_2dbm)_3$ (6). To a light pink stirred solution of $Mn(O_2CMe)_2 \cdot 4H_2O$ (55 mg, 0.22 mmol) in MeOH (10 mL) was added a purple solution of $NBu^n_4MnO_4$ (20 mg, 0.056 mmol) in MeOH (5 mL) to give a red-brown solution to which was added a solution of Me_2dbmH (212 mg, 0.84 mmol) in MeCN (20 mL). After a few minutes, the green precipitate that rapidly formed was collected by filtration, washed with Et_2O, and dried in vacuo. The yield was 68% based on Mn. Anal. Calcd (Found): C, 75.73 (75.83); H, 5.61 (5.64); N, 0.00 (0.00).

$MnCl(Et_2dbm)_2$ (7). To a solution of $MnCl_2 \cdot 4H_2O$ (110.8 mg, 0.56 mmol) in MeOH (3 mL) was added a purple solution of Bu_4NMnO_4 (50.6 mg, 0.14 mmol) in MeCN (6 mL). To the resulting red-brown solution was immediately added solid Et_2dbmH (392 mg, 1.4 mmol), the mixture stirred for about 45 min, and the solvents were evaporated to dryness. The residue was thoroughly washed with Et_2O, and the remaining solid was redissolved in CH_2Cl_2. A small amount of a white precipitate was removed by filtration, and the solvent was removed to dryness. The residue was washed with Et_2O and dried in vacuo. The yield was 56% based on Mn. Anal. Calcd (Found) for **7**·0.4 MeCN: C, 70.02 (69.96); H, 5.94 (6.00); N, 0.84 (0.86).

$MnBr(Et_2dbm)_2$ (8). Solid $MnBr_2 \cdot 4H_2O$ (0.15 g, 0.56 mmol) was dissolved in a stirred yellow solution of Et_2dbmH (0.39 g, 1.4 mmol) in MeCN (10 mL), followed by addition of a purple solution of $NBu^n_4MnO_4$ (51 mg, 0.14 mmol) in MeCN (5 mL). A microcrystalline solid soon started to precipitate, and after several more minutes, it was collected by filtration, washed with Et_2O, and dried in vacuo. The yield was 30% based on Mn. Anal. Calcd (Found) for **8**·0.1MeCN: C, 65.77 (65.63); H, 5.53 (5.53); N, 0.20 (0.16).

$Mn_6O_4Cl_4(Me_2dbm)_6$ (9). $MnCl(Me_2dbm)_2$ (**4**) (0.25 g, 0.42 mmol) was dissolved with stirring in a 1:1 mixture of $MeCN/CH_2Cl_2$ (32 mL). The solution was filtered and the filtrate allowed to concentrate by slow evaporation over a period of two weeks to give black, well-formed crystals (suitable for X-ray crystallography). These were collected by filtration, washed with EtOH to remove some white solid, and dried in vacuo. The yield was ~25% based on Mn. Anal. Calcd (Found) for **9**·$0.4CH_2Cl_2$: C, 59.21 (59.28); H, 4.41 (4.49); N, 0.00 (0.00). Crystals kept in contact with the mother liquor were identified crystallographically as **9**·$3CH_2Cl_2$.

$Mn_6O_4Br_4(Me_2dbm)_6$ (10). $MnBr(Me_2dbm)_2$ (**5**) (169 mg, 0.26 mmol) was dissolved with stirring in a 1:2 mixture of $MeCN/CH_2Cl_2$ (100 mL). The solution was filtered and the filtrate allowed to slowly concentrate by evaporation. After a few days, black, well-formed crystals (suitable for X-ray crystallography) had formed. They were isolated as for complex **9**. The yield was 12% based on Mn. Anal. Calcd (Found): C, 55.16 (55.06); H, 4.08 (4.11); N, 0.00 (0.00).

$Mn_6O_4Cl_4(Et_2dbm)_6$ (11). $MnCl(Et_2dbm)_2$ (**7**) (0.45 g, 0.64 mmol) was dissolved with stirring in MeCN (130 mL). The solution was filtered and the filtrate allowed to slowly concentrate by evaporation. After a few days, black, well-formed crystals had deposited. These were collected by filtration, washed with EtOH, and dried in vacuo. The yield was 25% based on Mn. Anal. Calcd (Found) for **11**·0.8MeCN: C, 61.86 (61.95); H, 5.23 (5.14); N, 0.50 (0.50).

$Mn_6O_4Br_4(Et_2dbm)_6$ (12). $MnBr(Et_2dbm)_2$ (**8**) (0.936 g, 1.35 mmol) was dissolved with stirring in MeCN (370 mL). The solution was filtered and the filtrate allowed to slowly concentrate by evaporation

(11) (a) Aubin, S. M. J.; Spagna, S.; Eppley, H. J.; Sager, R. E.; Folting, K.; Christou, G.; Hendrickson, D. N. *Mol. Cryst. Liq. Cryst.* **1997**, *305*, 181. (b) Eppley, H. J.; Aubin, S. M. J.; Wemple, M. W.; Adams, D. M.; Tsai, H.-L.; Grillo, V. A.; Castro, S. L.; Sun, Z.; Folting, K.; Huffman, J. C.; Hendrickson, D. N.; Christou, G. *Mol. Cryst. Liq. Cryst.* **1997**, *305*, 167.

(12) Barra, A. L.; Debrunner, P.; Gatteschi, D.; Schultz, C. E.; Sessolli, R. *Europhys. Lett.* **1996**, *35*, 133.

(13) Aromi, G.; Wemple, M. W.; Aubin, S. M. J.; Folting, K.; Hendrickson, D. N.; Christou, G. *J. Am. Chem. Soc.* **1998**, *120*, 2977.

(14) Vincent, J. B.; Folting, K.; Huffman, J. C.; Christou, G. *Inorg. Chem.* **1986**, *25*, 996.

Table 1. Crystallographic Data for Complexes **1**·CH_2Cl_2, **4**·CH_2Cl_2, **9**·$3CH_2Cl_2$, and **10**·CH_2Cl_2·MeCN

	1	**4**	**9**	**10**
formula[a]	$C_{31}H_{24}O_4Cl_3Mn$	$C_{35}H_{32}O_4Cl_3Mn$	$C_{105}H_{96}O_{16}Cl_{10}Mn_6$	$C_{105}H_{95}NO_{16}Cl_2Br_4Mn_6$
formula wt, g/mol	621.83	677.93	2298.06	2347.06
space group	$P2_1/n$	$C2/c$	$P2_1/c$	$P2_1/c$
a, Å	13.888(3)	24.802(5)	17.172(2)	17.180(6)
b, Å	8.348(1)	14.814(2)	18.302(2)	18.454(7)
c, Å	24.702(4)	17.458(3)	34.534(4)	34.636(14)
β, deg	102.69(1)	94.24(1)	100.36(1)	100.88(2)
V, Å^3	2794	6397	10677	10784
Z	8	8	4	4
T, °C	−168	−122	−171	−168
radiation, Å[b]	0.71069	0.71069	0.71069	0.71069
ρ_{calc}, g/cm^3	2.957	1.408	1.430	1.446
μ, cm^{-1}	15.548	6.850	9.726	22.775
$R(R_w)$, %	5.33 (4.56)	5.61 (4.32)	5.80 (5.73)	9.72 (6.25)

[a] Including solvate molecules. [b] Mo Kα, Graphite monochromator. [c] $R = 100\ \sum||F_o| - |F_c||/\sum|F_o|$. [d] $R_w = 100\ [\sum w(|F_o| - |F_c|)^2/\sum w|F_o|^2]^{1/2}$ where $w = 1/\sigma^2(|F_o|)$.

over 10 days. At the end of this period, black crystals suitable for X-ray crystallography had deposited and were collected by filtration, washed with EtOH, and dried in vacuo. The yield was 15% based on Mn. Anal. Calcd (Found): C, 57.31 (57.02); H, 4.81 (4.75); N, 0.00 (0.00).

X-ray Crystallography. Crystals suitable for crystallography were grown from CH_2Cl_2/Et_2O layerings (**1**·CH_2Cl_2 and **4**·CH_2Cl_2) or obtained directly from the preparative solution (**9**·$3CH_2Cl_2$ and **10**·CH_2Cl_2·MeCN). Suitable crystals were selected from the mother liquors, affixed to the tips of glass fibers with silicone grease, and transferred to the goniostat and cooled for characterization and data collection. The equipment employed was a Picker four-circle diffractometer; details of the diffractometry, low-temperature facilities, and computational procedures are available elsewhere.[15] After data collection ($+h$, $+k$, $\pm l$), correction for Lorentz and polarization effects and averaging of equivalent reflections, the structures were solved by direct methods (MULTAN or SHELXTL) and standard Fourier techniques and refined on F by full matrix, least-squares methods.

For complex **1**·CH_2Cl_2 ($6° \le 2\theta \le 50°$), a systematic search of a limited hemisphere of reciprocal space revealed monoclinic symmetry and systematic absences, indicating the unique monoclinic space group $P2_1/n$. Subsequent solution and refinement of the structure confirmed this choice. All non-hydrogen atoms were readily located and refined anisotropically; all hydrogen atoms were located in difference Fourier maps and refined isotropically in the final refinement cycles. The final difference Fourier map was essentially featureless, the largest peak being 1.03 e/Å^3 near the solvent molecule.

For complex **4**·CH_2Cl_2 ($6° \le 2\theta \le 50°$), a systematic search of a limited hemisphere of reciprocal space revealed monoclinic symmetry and systematic absences, corresponding to one of the monoclinic space groups, $C2/c$ or Cc. Subsequent solution and refinement of the structure confirmed centrosymmetric $C2/c$ to be the correct space group. All non-hydrogen atoms were readily located and refined anisotropically; hydrogen atoms were included in calculated positions as fixed atom contributors in the final refinement cycles. The structure contains molecules packed in sheets parallel to the [404] plane; the [404] reflection is the most intense by nearly a factor of 10. The final difference Fourier map was essentially featureless, the largest peak being 0.24 e/Å^3.

For complex **9**·$3CH_2Cl_2$ ($6° \le 2\theta \le 45°$), a systematic search of a limited hemisphere of reciprocal space revealed monoclinic symmetry and systematic absences corresponding to the unique space group $P2_1/c$. Subsequent solution and refinement of the structure confirmed this choice. All non-hydrogen atoms of the Mn_6 molecules were readily located and refined anisotropically; a total of three CH_2Cl_2 molecules were also located, two slightly disordered and one seriously disordered, involving several peaks with partial occupancy. Hydrogen atoms were included in calculated positions as fixed-atom contributors in the final refinement cycles. The final difference Fourier map was essentially featureless, the largest peak being 0.91 e/Å^3 near a disordered solvent molecule.

For complex **10**·CH_2Cl_2·MeCN ($6° \le 2\theta \le 45°$), a systematic search of a limited hemisphere of reciprocal space revealed monoclinic symmetry and systematic absences, corresponding to the unique space group $P2_1/c$. Subsequent solution and refinement of the structure confirmed this choice. All non-hydrogen atoms of the Mn_6 molecules were readily located and refined anisotropically; one MeCN and a badly disordered CH_2Cl_2 molecule were also located; a total of seven closely spaced peaks (C136−C142) suggested additional solvent molecules that were too badly disordered to be identified. Hydrogen atoms on the Mn_6 molecule were included in calculated positions as fixed-atom contributors. The final difference Fourier map was essentially featureless, the largest peaks being 0.8−1.3 e/Å^3 near the disordered solvent molecules.

Crystallographic data and final values of discrepancy indices $R(F)$ and $R_w(F)$ are listed in Table 1.

Physical Measurements. ^{1}H NMR spectra were collected on a 300 MHz Varian Gemini 2000 spectrometer and a 500 MHz Varian Inova spectrometer with the protio-solvent signal used as reference. IR and electronic spectra were recorded on KBr pellets and solutions, respectively, on Nicolet model 510P and Hewlett Packard model 8452A spectrophotometers, respectively. DC magnetic susceptibility data were collected on powdered, microcrystalline samples (restrained in eicosane to prevent torquing) on a Quantum Design MPMS5 SQUID magnetometer equipped with a 5.5 T (55 kG) magnet. A diamagnetic correction to the observed susceptibilities was applied using Pascal's constants. AC magnetic susceptibility measurements were made on a Quantum Design MPMS2 SQUID magnetometer equipped with a 1 T (10 kG) magnet and capable of achieving temperatures of 1.7 to 400 K. The AC field range is 1×10^{-4} to 5 G oscillating at a frequency in the range 5×10^{-4} to 1512 Hz. AC susceptibility data were collected on powdered, microcrystalline samples in an AC field of 1.0 G oscillating in the 0.74−1512 Hz range and in an applied DC field of 0−6.0 kG.

Results and Discussion

Syntheses. Entry into the new family of Mn_6 clusters is via the mononuclear, five-coordinate complexes $MnX(R_2dbm)_2$ (X = Cl^-, Br^-; R = Me, Et). The Cl^- monomers were originally obtained from the reactions of $[Mn_4O_2(O_2CMe)_6(py)_2(R_2dbm)_2]$ with 6 equiv. of the carboxylate-abstracting reagent Me_3SiCl, but more direct procedures were subsequently developed to the R = H (**1**), Me (**4**), and Et (**7**) species.

In the absence of a simple source of $MnCl_3$ stable in the solid state, Mn^{III} was generated in situ in MeCN/MeOH mixtures by oxidation of $MnCl_2$ with MnO_4^- in a 4:1 ratio (eq 1). This gave

$$4Mn^{II} + Mn^{VII} \rightarrow 5\ Mn^{III} \qquad (1)$$

a brown solution from which deposited the desired [MnCl-

(15) Chisholm, M. H.; Folting, K.; Huffman, J. C.; Kirkpatrick, C. C. *Inorg. Chem.* **1984**, *23*, 1021.

$(R_2dbm)_2$] species on addition of R_2dbmH (eq 2). This one-pot

$$4\ MnCl_2 + MnO_4^- + 10\ R_2dbmH \rightarrow 5\ MnCl(R_2dbm)_2 + 4\ H_2O + 3\ Cl^- + 2\ H^+ \quad (2)$$

procedure can be readily extended to the preparation of the $[MnBr(R_2dbm)_2]$ complexes **2**, **5**, and **8** by use of $MnBr_2$ in place of $MnCl_2$.

The six-coordinate, tris-chelate complexes $[Mn(dbm)_3]$ (**3**) and $[Mn(Me_2dbm)_3]$ (**6**) were required to assist with spectroscopic assignments in the formation of the Mn_6 species, and they were prepared by a procedure similar to that employed for the $[MnX(R_2dbm)_2]$ complexes, i.e., using Mn^{II}/MnO_4^- to generate Mn^{III} in situ followed by the addition of 3 equiv of R_2dbmH (eq 3).

$$4\ Mn(O_2CMe)_2 + MnO_4^- + 15\ R_2dbmH \rightarrow 5\ Mn(R_2dbm)_3 + 4\ H_2O + 7\ MeCO_2H + MeCO_2^- \quad (3)$$

The conversion of $[MnCl(Me_2dbm)_2]$ (**4**) to $[Mn_6O_4Cl_4(Me_2dbm)_6]$ (**9**) was first realized in a solution of **4** in CH_2Cl_2/MeCN (1:1), which slowly deposited black crystals of **9** over the course of two weeks. Yields of $\leq$25% have been obtained. The source of the oxide ions in **9** is undoubtedly H_2O, suggesting that the formation of the hexanuclear product involves hydrolysis of the mononuclear species, facilitated by the Brønsted basicity of Me_2dbm^- (eq 4). The overall transformation is not as simple

$$6\ MnCl(Me_2dbm)_2 + 4\ H_2O \rightarrow [Mn_6O_4Cl_4(Me_2dbm)_6] + 6\ Me_2dbmH + 2\ HCl \quad (4)$$

as this equation suggests, however: IR spectral examination of solid obtained from the filtrate by solvent removal shows the presence of $Mn(Me_2dbm)_3$ (**6**) as well as other undefined species. Thus, the reaction solution probably contains several species in equilibrium, and the isolation of pure **9** is probably due to its low solubility in this solvent mixture. Analogous slow hydrolysis reactions of $[MnCl(Et_2dbm)_2]$ (**7**) were subsequently found to yield the corresponding complex $[Mn_6O_4Cl_4(Et_2dbm)_6]$ (**11**). Interestingly, however, analogous solutions of $[MnCl(dbm)_2]$ (**1**) do not produce $[Mn_6O_4Cl_4(dbm)_6]$ on standing or any other related material. If this complex is among the species present in solution, it must be too soluble to crystallize. Attempts to prepare it by altering reaction conditions have not been pursued.

The identification of a novel $[Mn_6(\mu_3\text{-}O)_4(\mu_3\text{-}Cl)_4]^{6+}$ core in **9** (vide infra) raised the question of whether the corresponding Br^- complexes might be attainable, and this was subsequently shown to be the case. The $[MnBr(R_2dbm)_2]$ complexes **2**, **5**, and **8** can be prepared in a fashion very similar to that for the Cl^- species by using $MnBr_2$, and subsequent slow hydrolysis in $MeCN/CH_2Cl_2$ (1:2) or MeCN gave $[Mn_6O_4Br_4(R_2dbm)_6]$ (R = Me, **10**; R = Et, **12**). Again, the dbm complex **2** did not yield a Mn_6 crystalline solid. Attempts are in progress to extend the $[Mn_6O_4X_4]^{6+}$ family to F^- and other similar anionic ligands (RO^-, N_3^-, etc.).

Description of Structures. Labeled ORTEP plots of complexes **1** and **4** are presented in Figure 1, and selected interatomic distances and angles are listed in Tables 2 and 3. The two complexes are very similar and comprise a five-coordinate Mn^{III} ligated to two chelate groups (Mn−O ≈ 1.89 Å) and a Cl^- ion (Mn−Cl ≈ 2.37 Å. The geometry is square-pyramidal (τ is 0.05 and 0.06 for **1** and **4**, respectively, where $\tau = 0$ and 1 for perfect square-pyramidal and trigonal bipyramidal geometries, respectively)[16] with the Cl^- ion in the apical position. The complexes possess virtual C_{2v} symmetry. Inspection of packing diagrams shows interesting supramolecular architecture: for both **1** and **4**, the molecules align face-to-face in a zigzag fashion (side view shown)

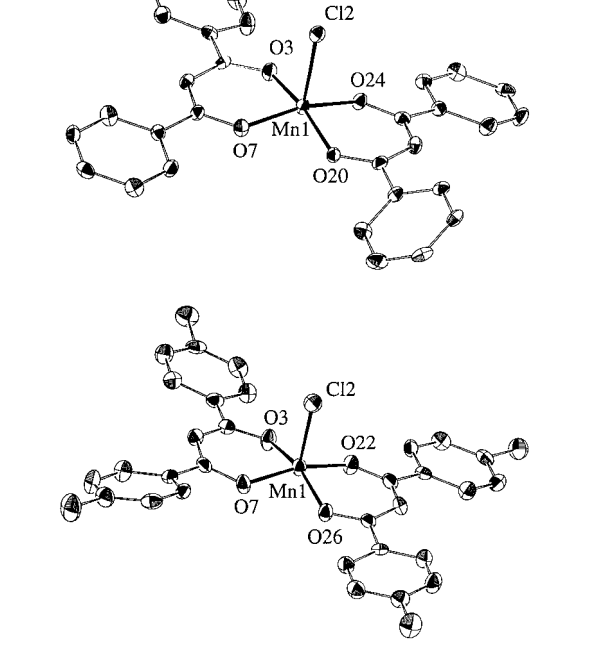

Figure 1. ORTEP representation (50% probability ellipsoids) of $[MnCl(dbm)_2$ (**1**, top) and $[MnCl(Me_2dbm)_2]$ (**4**, bottom).

Table 2. Selected Bond Distances (Å) and Angles (deg) for $[MnCl(dbm)_2]$ (**1**)

Mn(1)−Cl(2)	2.374(2)	Mn(1)−O(20)	1.895(3)
Mn(1)−O(3)	1.896(3)	Mn(1)−O(24)	1.901(3)
Mn(1)−O(7)	1.896(3)		
Cl(2)−Mn(1)−O(3)	98.64(12)	O(3)−Mn(1)−O(20)	164.81(15)
Cl(2)−Mn(1)−O(7)	98.96(11)	O(3)−Mn(1)−O(24)	85.91(14)
Cl(2)−Mn(1)−O(20)	96.53(11)	O(7)−Mn(1)−O(20)	88.00(14)
Cl(2)−Mn(1)−O(24)	98.92(11)	O(7)−Mn(1)−O(24)	162.08(15)
O(3)−Mn(1)−O(7)	90.28(14)	O(20)−Mn(1)−O(24)	91.11(14)

Table 3. Selected Bond Distances (Å) and Angles (deg) for $[MnCl(Me_2dbm)_2]$ (**4**)

Mn(1)−Cl(2)	2.380(2)	Mn(1)−O(22)	1.887(3)
Mn(1)−O(3)	1.897(3)	Mn(1)−O(26)	1.890(3)
Mn(1)−O(7)	1.895(3)		
Cl(2)−Mn(1)−O(3)	102.65(11)	O(3)−Mn(1)−O(22)	86.35(12)
Cl(2)−Mn(1)−O(7)	95.90(11)	O(3)−Mn(1)−O(26)	160.19(15)
Cl(2)−Mn(1)−O(22)	100.58(11)	O(7)−Mn(1)−O(22)	163.51(15)
Cl(2)−Mn(1)−O(26)	97.14(11)	O(7)−Mn(1)−O(26)	86.92(12)
O(3)−Mn(1)−O(7)	90.22(13)	O(22)−Mn(1)−O(26)	90.85(13)

to give a one-dimensional double ribbon held together by π-stacking interactions between the R_2dbm groups. These double ribbons are stacked on top of each other to form a sheet, which then stacks to give the 3D structure. In **4**, these sheets all have the ribbon directions parallel, whereas, in **1**, adjacent sheets have

(16) Addison, A. W.; Rao, T. N.; Reedijk, J.; Rijn, J.; Verschoor, G. C. *J. Chem. Soc., Dalton Trans.* **1984**, 1349.

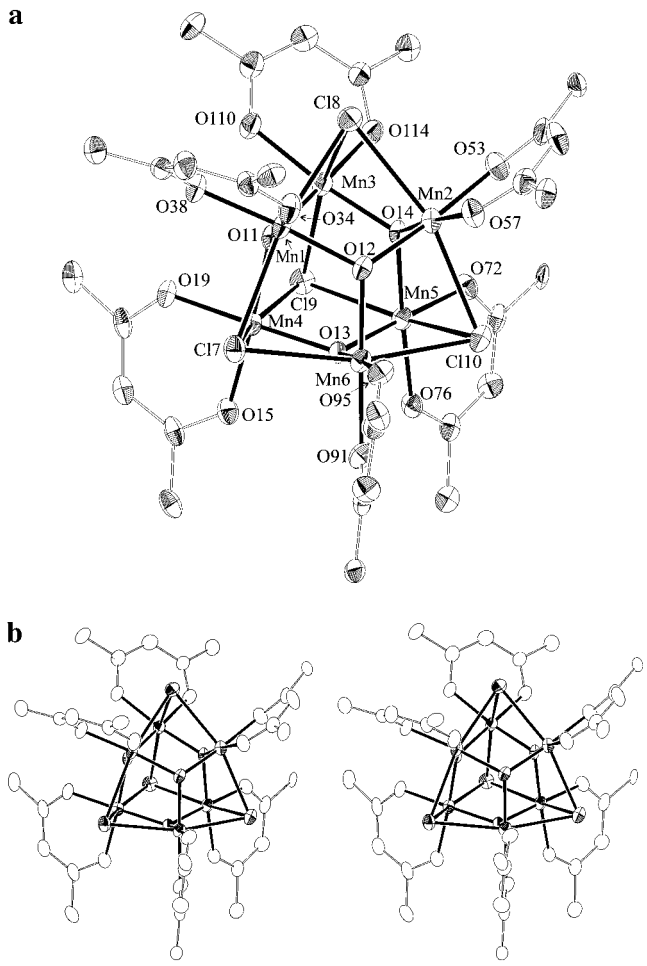

Figure 2. ORTEP representation (50% probability ellipsoids) and stereopair of $[Mn_6O_4Cl_4(Me_2dbm)_6]$ (**9**) from a viewpoint that emphasizes the near tetrahedron; for clarity, only the ipso C atom of each aromatic ring is shown.

perpendicular ribbon directions. Packing diagrams are available as Supporting Information.

The structures of **9** and **10** are shown in Figures 2−4, and selected interatomic distances and angles are listed in Tables 4 and 5, with the most important parameters compared in Table 6. The structure of **9** consists of a Mn_6^{III} octahedron (Figure 4) with four nonadjacent faces bridged by μ_3-O^{2-} ions and the other four faces bridged by μ_3-Cl^- ions. Six-coordinate, approximately octahedral geometry at each metal is completed by a chelating Me_2dbm group. The Cl^- ions possess trigonal pyramidal coordination geometry with a sum-of-angles (soa) of ∼223°, but the O^{2-} ions are almost trigonal planar with a soa of ∼349°, and they lie only ∼0.37 Å above the Mn_3 plane which they bridge. As expected for high-spin Mn^{III} (d^4) in near-octahedral geometry, there is a Jahn−Teller (JT) distortion, and it takes the form of an axial elongation of the two trans Mn−Cl bonds, making them unusually long (2.618(3)−2.692(3) Å). In contrast, the Mn−O^{2-} (1.876(4)−1.899(5) Å) and Mn−O(Me_2dbm) (1.903(5)−1.925(5) Å) bond lengths are as expected. As a result of (i), the long Mn−Cl vs short Mn−O^{2-} bonds and (ii) trigonal planar vs trigonal pyramidal geometry at the O^{2-} and Cl^- ions, respectively, the $[Mn_6O_4Cl_4]^{6+}$ core is a near tetrahedron with a Cl^- at each vertex, a Mn at the midpoint of each edge, and an O^{2-} bridging each face. The cluster has virtual T_d symmetry.

Complex **10** is isostructural with **9**, the only difference being the Br^--for-Cl^- substitution; the coordination geometries at Mn,

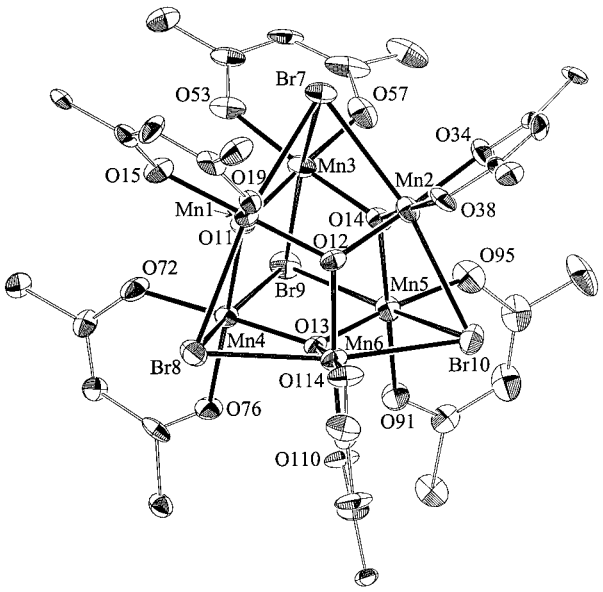

Figure 3. ORTEP representation (50% probability ellipsoids) of $[Mn_6O_4Br_4(Me_2dbm)_6]$ (**10**); for clarity, only the ipso C atom of each aromatic ring is shown.

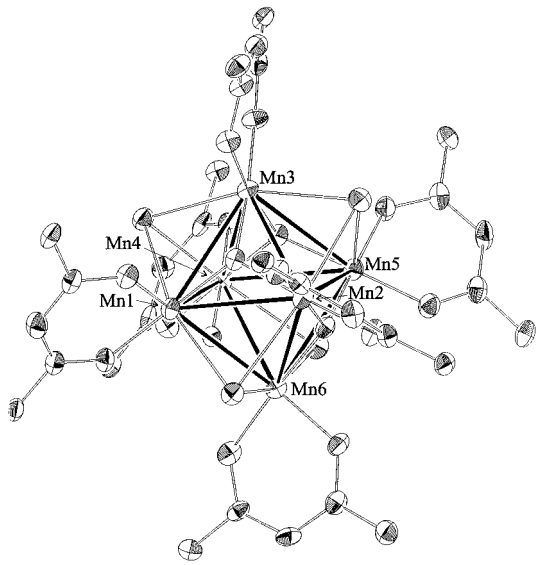

Figure 4. ORTEP representation (50% probability ellipsoids) of $[Mn_6O_4Cl_4(Me_2dbm)_6]$ (**9**) with Mn−Mn vectors shown to emphasize the Mn_6 octahedron.

Br^-, and O^{2-} and the location of the JT axes are the same. In Table 6 are collected the metric parameters for the $[Mn_6O_4X_4]^{6+}$ cores of **9** and **10**, and it can be seen that only small differences exist. The main difference is in the Mn−Br (av 2.789 Å) vs Mn−Cl (av 2.653 Å) bond lengths, the difference of 0.136 Å being comparable to the 0.15 Å difference in ionic (and covalent) radii for six-coordinate Br^-/Cl^-.[17] In $[Mn_4O_3X(O_2CMe)_3(dbm)_3]$ (X = Cl^-, Br^-),[18] where the X^- ions are μ_3-bridging Mn_3^{III} triangles as in **9** and **10**, the Mn−Br (2.803 Å) vs Mn−Cl (2.650 Å) average bond difference is 0.15 Å. The longer Mn−Br vs Mn−Cl bonds in **9**/**10** lead to expected changes in core angles, i.e., the Mn−Br−Mn angles are smaller (av 70.3°) than Mn−Cl−Mn angles (74.3°), and Br−Mn−Br angles (167.2°) are larger than Cl−Mn−Cl angles (162.1°). It

(17) Shannon, R. D. *Acta Crystallogr., Sect. A* **1976**, *A32*, 751.
(18) Wang, S.; Tsai, H.-L.; Libby, E.; Folting, K.; Streib, W. E.; Hendrickson, D. N.; Christou, G. *Inorg. Chem.* **1996**, *35*, 7578.

Table 4. Selected Interatomic Distances (Å) and Angles (deg) for $[Mn_6O_4Cl_4(Me_2dbm)_6]$ (**9**)

Mn(1)··Mn(2)	3.195(2)	Mn(4)··Mn(5)	3.205(2)	Mn(2)−Cl(8)	2.644(3)		
Mn(1)··Mn(3)	3.207(2)	Mn(4)··Mn(6)	3.199(2)	Mn(1)−O(11)	1.880(4)	Mn(2)−O(57)	1.910(5)
Mn(4)··Mn(4)	3.203(2)	Mn(5)··Mn(6)	3.221(2)	Mn(1)−O(12)	1.876(4)	Mn(3)−O(11)	1.885(4)
Mn(1)··Mn(6)	3.193(2)	Mn(1)··Mn(5)	4.526(2)	Mn(1)−O(34)	1.927(5)	Mn(3)−O(14)	1.877(4)
Mn(2)··Mn(3)	3.199(2)	Mn(2)··Mn(4)	4.534(2)	Mn(1)−O(38)	1.918(5)	Mn(3)−O(110)	1.910(5)
Mn(2)··Mn(5)	3.210(2)	Mn(3)··Mn(6)	4.532(2)	Mn(2)−O(12)	1.899(5)	Mn(3)−O(114)	1.918(5)
Mn(2)··Mn(6)	3.219(2)	Mn(3)−Cl(8)	2.692(3)	Mn(2)−O(14)	1.886(4)	Mn(4)−O(11)	1.881(5)
Mn(3)··Mn(4)	3.204(2)	Mn(3)−Cl(9)	2.651(3)	Mn(2)−O(53)	1.903(5)	Mn(4)−O(13)	1.895(4)
Mn(3)··Mn(5)	3.189(2)	Mn(4)−Cl(9)	2.638(3)	Mn(4)−O(15)	1.921(5)	Mn(5)−O(76)	1.905(5)
Mn(1)−Cl(7)	2.662(3)	Mn(5)−Cl(9)	2.623(3)	Mn(4)−O(19)	1.922(5)	Mn(6)−O(12)	1.894(5)
Mn(4)−Cl(7)	2.675(3)	Mn(2)−Cl(10)	2.618(3)	Mn(5)−O(13)	1.887(4)	Mn(6)−O(13)	1.890(5)
Mn(6)−Cl(7)	2.652(3)	Mn(5)−Cl(10)	2.666(3)	Mn(5)−O(14)	1.885(5)	Mn(6)−O(91)	1.922(5)
Mn(1)−Cl(8)	2.652(3)	Mn(6)−Cl(10)	2.658(3)	Mn(5)−O(72)	1.909(5)	Mn(6)−O(95)	1.915(5)

O(11)−Mn(1)−O(12)	93.24(19)	O(110)−Mn(3)−O(114)	89.00(20)	O(13)−Mn(6)−O(95)	177.24(21)	O(91)−Mn(6)−O(95)	89.49(21)
O(11)−Mn(1)−O(34)	175.84(21)	O(11)−Mn(4)−O(13)	92.39(19)	Mn(1)−Cl(7)−Mn(4)	73.77(20)	Mn(3)−Cl(9)−Mn(4)	74.57(20)
O(11)−Mn(1)−O(38)	87.14(19)	O(11)−Mn(4)−O(15)	176.38(19)	Mn(1)−Cl(7)−Mn(6)	73.87(20)	Mn(3)−Cl(9)−Mn(5)	74.42(20)
O(12)−Mn(1)−O(34)	90.34(20)	O(11)−Mn(4)−O(19)	87.91(20)	Mn(4)−Cl(7)−Mn(6)	73.82(20)	Mn(4)−Cl(9)−Mn(5)	75.05(20)
O(12)−Mn(1)−O(38)	176.19(21)	O(13)−Mn(4)−O(15)	90.82(19)	Mn(1)−Cl(8)−Mn(2)	74.21(20)	Mn(2)−Cl(10)−Mn(5)	74.80(20)
O(34)−Mn(1)−O(38)	89.43(20)	O(13)−Mn(4)−O(19)	175.85(21)	Mn(1)−Cl(8)−Mn(3)	73.75(20)	Mn(2)−Cl(10)−Mn(6)	75.19(20)
O(12)−Mn(2)−O(14)	93.64(19)	O(15)−Mn(4)−O(19)	89.02(20)	Mn(2)−Cl(8)−Mn(3)	73.68(20)	Mn(5)−Cl(10)−Mn(6)	74.45(20)
O(12)−Mn(2)−O(53)	175.17(21)	O(13)−Mn(5)−O(14)	93.28(19)	Mn(1)−O(11)−Mn(3)	116.79(23)	Mn(4)−O(13)−Mn(5)	115.89(23)
O(12)−Mn(2)−O(57)	89.25(20)	O(13)−Mn(5)−O(72)	177.94(20)	Mn(1)−O(11)−Mn(4)	116.79(23)	Mn(4)−O(13)−Mn(6)	115.39(23)
O(14)−Mn(2)−O(53)	88.18(20)	O(13)−Mn(5)−O(76)	88.85(19)	Mn(3)−O(11)−Mn(4)	116.61(22)	Mn(5)−O(13)−Mn(6)	117.04(23)
O(14)−Mn(2)−O(57)	174.43(20)	O(14)−Mn(5)−O(72)	88.63(20)	Mn(1)−O(12)−Mn(2)	115.61(23)	Mn(2)−O(14)−Mn(3)	116.46(23)
O(53)−Mn(2)−O(57)	89.33(21)	O(14)−Mn(5)−O(76)	176.99(20)	Mn(1)−O(12)−Mn(6)	115.74(23)	Mn(2)−O(14)−Mn(5)	116.66(23)
O(11)−Mn(3)−O(14)	92.28(19)	O(72)−Mn(5)−O(76)	89.28(20)	Mn(2)−O(12)−Mn(6)	116.10(22)	Mn(3)−O(14)−Mn(5)	115.96(23)
O(11)−Mn(3)−O(110)	89.82(20)	O(12)−Mn(6)−O(13)	93.91(19)	Cl(7)−Mn(1)−Cl(8)	163.23(23)	Cl(7)−Mn(4)−Cl(9)	162.06(23)
O(11)−Mn(3)−O(114)	175.63(21)	O(12)−Mn(6)−O(91)	177.32(20)	Cl(8)−Mn(2)−Cl(10)	162.77(23)	Cl(9)−Mn(5)−Cl(10)	161.29(23)
O(14)−Mn(3)−O(110)	172.42(21)	O(12)−Mn(6)−O(95)	87.98(20)	Cl(8)−Mn(3)−Cl(9)	161.35(23)	Cl(7)−Mn(6)−Cl(10)	161.85(23)
O(14)−Mn(3)−O(114)	89.43(20)	O(13)−Mn(6)−O(91)	88.65(20)				

Table 5. Selected Interatomic Distances (Å) and Angles (deg) for $[Mn_6O_4Br_4(Me_2dbm)_6]$ (**10**)

Mn(1)··Mn(2)	3.200(4)	Mn3··Mn6	4.546(4)	Mn(2)··Mn(4)	4.541(4)		
Mn(1)··Mn(3)	3.217(4)	Mn(1)−Br(7)	2.791(2)	Mn(1)−O(11)	1.892(9)	Mn(2)−O(38)	1.930(8)
Mn(1)··Mn(4)	3.223(4)	Mn(2)−Br(7)	2.809(2)	Mn(1)−O(12)	1.896(8)	Mn(3)−O(11)	1.871(8)
Mn(1)··Mn(6)	3.231(4)	Mn(3)−Br(7)	2.799(2)	Mn(1)−O(15)	1.915(8)	Mn(3)−O(14)	1.892(8)
Mn(2)··Mn(3)	3.215(4)	Mn(1)−Br(8)	2.794(2)	Mn(1)−O(19)	1.921(8)	Mn(3)−O(53)	1.911(9)
Mn(2)··Mn(5)	3.216(4)	Mn(4)−Br(8)	2.828(2)	Mn(2)−O(12)	1.866(8)	Mn(3)−O(57)	1.901(9)
Mn(2)··Mn(6)	3.195(4)	Mn(6)−Br(8)	2.762(2)	Mn(2)−O(14)	1.880(8)	Mn(4)−O(11)	1.908(8)
Mn(3)··Mn(4)	3.218(4)	Mn(3)−Br(9)	2.770(2)	Mn(2)−O(34)	1.912(8)	Mn(4)−O(13)	1.874(8)
Mn(3)··Mn(5)	3.207(4)	Mn(4)−Br(9)	2.749(2)	Mn(4)−O(72)	1.903(9)	Mn(5)−O(95)	1.909(9)
Mn(4)··Mn(5)	3.197(4)	Mn(5)−Br(9)	2.786(2)	Mn(4)−O(76)	1.929(8)	Mn(6)−O(12)	1.920(8)
Mn(4)··Mn(6)	3.223(4)	Mn(2)−Br(10)	2.789(2)	Mn(5)−O(13)	1.860(8)	Mn(6)−O(13)	1.922(8)
Mn(5)··Mn(6)	3.198(4)	Mn(5)−Br(10)	2.824(2)	Mn(5)−O(14)	1.889(8)	Mn(6)−O(110)	1.921(8)
Mn(1)··Mn(5)	4.535(4)	Mn(6)−Br(10)	2.770(2)	Mn(5)−O(91)	1.914(8)	Mn(6)−O(114)	1.906(9)

O(11)−Mn(1)−O(12)	93.3(3)	O(11)−Mn(4)−O(13)	92.2(3)	Mn(1)−O(11)−Mn(3)	116.9(4)	Mn(4)−O(13)−Mn(5)	117.8(4)
O(11)−Mn(1)−O(15)	89.2(3)	O(11)−Mn(4)−O(72)	88.9(4)	Mn(1)−O(11)−Mn(4)	116.0(4)	Mn(4)−O(13)−Mn(6)	116.2(4)
O(11)−Mn(1)−O(19)	176.5(4)	O(11)−Mn(4)−O(76)	178.1(4)	Mn(3)−O(11)−Mn(4)	116.7(4)	Mn(5)−O(13)−Mn(6)	115.5(4)
O(12)−Mn(1)−O(15)	177.4(4)	O(13)−Mn(4)−O(72)	178.7(4)	Mn(1)−O(12)−Mn(2)	116.6(4)	Mn(2)−O(14)−Mn(3)	116.9(4)
O(12)−Mn(1)−O(19)	88.2(3)	O(13)−Mn(4)−O(76)	89.2(3)	Mn(1)−O(12)−Mn(6)	115.7(4)	Mn(2)−O(14)−Mn(5)	117.1(4)
O(15)−Mn(1)−O(19)	89.2(3)	O(72)−Mn(4)−O(76)	89.6(4)	Mn(2)−O(12)−Mn(6)	115.1(4)	Mn(3)−O(14)−Mn(5)	116.1(4)
O(12)−Mn(2)−O(14)	93.3(3)	O(13)−Mn(5)−O(14)	92.3(3)	Mn(1)−Br(7)−Mn2	69.70(4)	Mn(4)−Br(9)−Mn(5)	70.57(4)
O(12)−Mn(2)−O(34)	176.5(4)	O(13)−Mn(5)−O(91)	89.8(3)	Mn(1)−Br(7)−Mn(3)	70.02(4)	Mn(2)−Br(10)−Mn(5)	69.89(4)
O(12)−Mn(2)−O(38)	89.5(3)	O(13)−Mn(5)−O(95)	173.9(4)	Mn(2)−Br(7)−Mn(3)	69.96(4)	Mn(2)−Br(10)−Mn(6)	70.15(4)
O(14)−Mn(2)−O(34)	87.7(4)	O(14)−Mn(5)−O(91)	176.0(4)	Mn(1)−Br(8)−Mn(4)	69.95(4)	Mn(5)−Br(10)−Mn(6)	69.72(4)
O(14)−Mn(2)−O(38)	176.7(4)	O(14)−Mn(5)−O(95)	89.4(4)	Mn(1)−Br(8)−Mn(6)	71.11(4)	Br(8)−Mn(4)−Br(9)	166.1(4)
O(34)−Mn(2)−O(38)	89.6(4)	O(91)−Mn(5)−O(95)	88.8(4)	Mn(4)−Br(8)−Mn(6)	70.41(4)	Br(9)−Mn(5)−Br(10)	166.4(4)
O(11)−Mn(3)−O(14)	91.7(4)	O(12)−Mn(6)−O(13)	93.1(3)	Mn(3)−Br(9)−Mn(4)	71.33(4)	Br(8)−Mn(6)−Br(10)	168.3(4)
O(11)−Mn(3)−O(53)	91.4(4)	O(12)−Mn(6)−O(110)	175.7(4)	Mn(3)−Br(9)−Mn(5)	70.53(4)		
O(11)−Mn(3)−O(57)	176.0(4)	O(12)−Mn(6)−O(114)	88.8(3)	Br(7)−Mn(1)−Br(8)	167.3(4)		
O(14)−Mn(3)−O(53)	176.4(4)	O(13)−Mn(6)−O(110)	89.1(3)	Br(7)−Mn(2)−Br(10)	167.9(4)		
O(14)−Mn(3)−O(57)	87.4(4)	O(13)−Mn(6)−O(114)	175.6(4)	Br(7)−Mn(3)−Br(9)	167.2(4)		
O(53)−Mn(3)−O(57)	89.6(4)	O(110)−Mn(6)−O(114)	89.2(4)				

is interesting to note, however, that other bond distances and angles in the core are (essentially) unaffected by the Br^--for-Cl^- substitution. This will be of relevance to the magnetochemical discussion (vide infra).

Although many $[M_6(\mu_3\text{-}X)_8]$ face-capped metal octahedra are known,[19] only a relative few contain two types of X group, e.g., the $[Ti_6O_4Cl_4]$,[20] $[Ti_6O_6Cl_2]$,[20] $[Ti_6Te_6O_2]$,[21] and $[Re_6Y_xZ_{8-x}]$ ($x = 5$, Y = S or Se, Z = Cl; $x = 6$, Y = S, Z = Cl)[22] cores. Only the $[Ti_6(\mu_3\text{-}O)_4(\mu_3\text{-}Cl)_4]$ core of $[(C_5H_5Me)_6Ti_6O_4Cl_4]$[20] contains, as **9**, four O^{2-} and four Cl^- bridges, but the structure

(19) Lee, S. L.; Holm, R. H. *Angew. Chem., Int. Ed. Engl.* **1990**, *29*, 840 and references therein.

(20) (a) Roth, A.; Floriani, C.; Chiesi-Villa, A.; Guastini, C. *J. Am. Chem. Soc.* **1986**, *108*, 6823. (b) Carofiglio, T.; Floriani, C.; Roth, A.; Sgamellotti, A.; Rosi, M.; Chiesi-Villa, A.; Rizzoli, C. *J. Organomet. Chem.* **1995**, *488*, 141.

(21) Gindelberger, D. E. *Acta Crystallogr., Sect. C* **1996**, *52*, 2493.

Table 6. Comparison of the $[Mn_6O_4X_4]^{6+}$ Core Parameters (Å, deg) of **9** (X = Cl) and **10** (X = Br)

	Cl[a]	Br[a]
Mn···Mn[b]	3.204(9)	3.212(11)
Mn··Mn[c]	4.531(3)	4.541(4)
Mn−X	2.653(20)	2.789(23)
Mn−O[d]	1.886(7)	1.889(2)
X−Mn−X	162.1(7)	167.2(8)
O−Mn−O	93.1(6)	92.7(6)
Mn−O−Mn	116.3(5)	116.4(7)
Mn−X−Mn	74.3(5)	70.3(5)

[a] Averaged using virtual T_d symmetry; numbers in parentheses are the standard deviation from the mean. [b] Adjacent atoms. [c] Opposite atoms. [d] μ_3-O atoms.

Table 7. ^{1}H NMR Spectral Data[a] for Complexes **1**−**12**

complex	chemical shift/ppm[b,c]
$[MnCl(dbm)_2]$ (**1**)	5.4 (*m*), 2.08 (*p*), 54.7 (CH)
$[MnBr(dbm)_2]$ (**2**)	5.6 (*m*), 2.04 (*p*), 58.6 (CH)
$[Mn(dbm)_3]$ (**3**)	5.8 (*o*), 8.00 (*m*), 3.63 (*p*), 23.4 (CH)
$[MnCl(Me_2dbm)_2]$ (**4**)	5.1 (*m*), 57.6 (CH), 1037 (Me)
$[MnBr(Me_2dbm)_2]$ (**5**)	5.3 (*m*), 59.9 (CH), 10.88 (Me)
$[Mn(Me_2dbm)_3]$ (**6**)	5.5 (*o*), 7.76 (*m*), 24.0 (CH), 7.47 (Me)
$[MnCl(Et_2dbm)_2]$ (**7**)	5.1 (*m*), 60 (CH), 9.09 (CH_2), 1.36 (Me)
$[MnBr(Et_2dbm)_2]$ (**8**)	5.4 (*m*), 63 (CH), 9.48 (CH_2), 1.49 (Me)
$[Mn_6O_4Cl_4(Me_2dbm)_6]$ (**9**)	3.9 (*m*), 80−85 (CH),[d] 18.15 (Me)
$[Mn_6O_4Br_4(Me_2dbm)_6]$ (**10**)	∼4 (*m*),[e] 80−85 (CH),[d] 18.18 (Me)
$[Mn_6O_4Cl_4(Et_2dbm)_6]$ (**11**)	4.0 (*m*), ∼83 (CH), 15.07 (CH_2), 1.15 (Me)
$[Mn_6O_4Br_4(Et_2dbm)_6]$ (**12**)	4.3 (*m*), ∼83 (CH), 14.97 (CH_2), 1.27 (Me)

[a] In $CDCl_3$ at ∼23 °C. [b] On the δ scale; shifts downfield are positive. [c] Very broad signals are given to 1 decimal place (±0.2 ppm) or to the nearest integer (±1 ppm); other signals are to two decimal places and are ±0.05 ppm. [d] Poorly defined. [e] Poorly defined; in CD_2Cl_2, δ = 4.1 ppm.

does not approximate to a tetrahedron. $[Mn^{III}_6X_8]$ octahedral species have been unknown to date, although a $[Mn_6(\mu_3\text{-}O)_4(\mu_3\text{-}X)_4]^{4+}$ unit as found in **9** and **10** but at the $2Mn^{II}$, $4Mn^{III}$ level is also a recognizable fragment within the higher nuclearity clusters $[Mn_{10}O_4X_{12}(biphen)_4]^{4-}$ (biphen = 2,2′-biphenoxide).[4d] In the latter, four additional Mn^{II} atoms are attached to the core O^{2-} ions, making them μ_4.

^{1}H NMR Spectroscopy. ^{1}H NMR spectroscopy is a convenient and useful method to probe the solution behavior of paramagnetic species. In the present case, an important question to be addressed was whether the Mn_6 clusters retain their structure on dissolution. Complexes **1**−**12** are all soluble to a sufficient extent in CH_2Cl_2 and $CHCl_3$, and NMR spectra were recorded both in CD_2Cl_2 and $CDCl_3$. The obtained data were very similar in the two solvents, and only the $CDCl_3$ data will be detailed. The ^{1}H NMR data are collected in Table 7, and representative spectra for the bromo complexes **8** and **12** are presented in Figure 5. Peak assignments were made by consideration of peak integrations, the relative broadnesses, and the effect of Me or Et substitution at the para position of the dbm^- phenyl rings.

The complexes are all highly paramagnetic, and the NMR resonances are thus greatly shifted and broadened compared with those of a diamagnetic system. The spectrum for **8** in Figure 5 (top) shows a very broadened CH resonance at ∼63 ppm, (broadness $\propto r^{-6}$, where r is the Mn−H distance). The ortho hydrogens on the Et_2dbm ligands are broadened beyond detection and could not be safely located in any of the $MnX(R_2dbm)_2$ complexes; only in the $Mn(R_2dbm)_3$ complexes could very broad *o*-H resonances be detected at ∼5.8 ppm. The

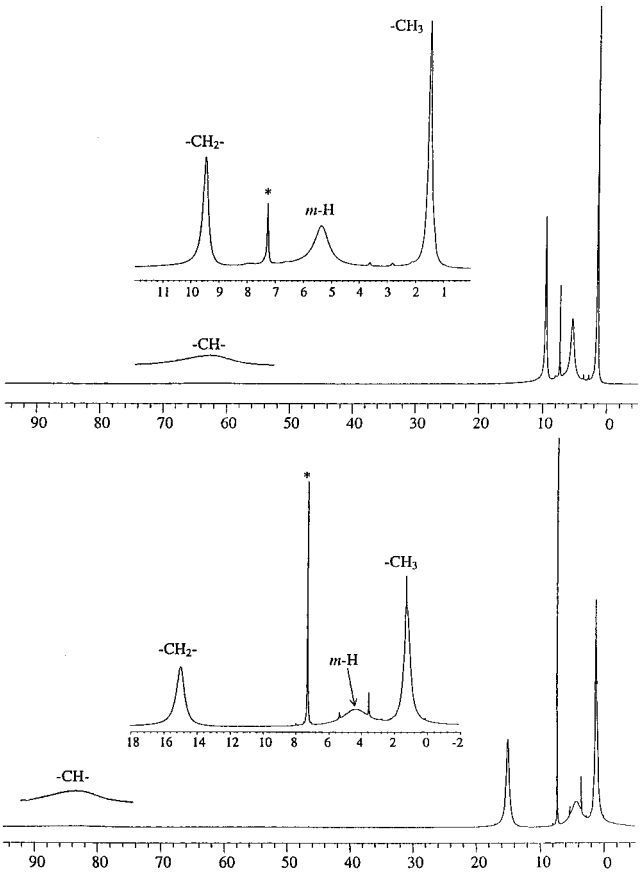

Figure 5. 500 MHz ^{1}H NMR spectra in $CDCl_3$ of $[MnBr(Et_2dbm)_2]$ (**8**, top) and $[Mn_6O_4Br_4(Et_2dbm)_6]$ (**12**, bottom); the insets are expansion of the indicated regions.

paramagnetic shifts for the R_2dbm ligands from their diamagnetic positions are all greater for the $MnX(R_2dbm)_2$ complexes than for the $Mn(R_2dbm)_3$ complexes (e.g., compare **1**/**2** with **3**, and **4**/**5** with **6**) even though they both contain S = 2 Mn^{III} ions. This is possibly due to greater spin delocalization onto each of two rather than three R_2dbm ligands in the five-coordinate complexes and perhaps greater dipolar contributions to the observed shifts in the lower symmetry five-coordinate complexes.

The Mn_6 complexes **9**−**12** all show very similar NMR spectra. The spectrum for **12** in Figure 5 (bottom) displays a CH resonance even more broadened and shifted to ∼83 ppm, and the other peaks also show slightly greater line widths than the mononuclear species. The *o*-H resonances are again broadened beyond detection. The appearance of only one set of R_2dbm resonances is consistent with effective T_d symmetry in solution and thus supports retention of the solid-state structure on dissolution. It had been suspected that any fragmentation of the Mn_6 clusters would likely yield $MnX(R_2dbm)_2$ and/or $Mn(R_2dbm)_3$ as at least some of the products, but no evidence of these or other species was observed in the NMR spectra. The NMR results thus suggest that structural integrity is retained on dissolution, and this in turn suggests the feasibility of further reactivity investigations on the $[Mn_6O_4X_4]$ cores. The results on the Mn_6 complexes are as found for many other $[Mn_xO_y]$ clusters[2,18] where the oxide bridges serve to help retain the structure on dissolution, at least in MeCN and chlorinated hydrocarbon solvents.

DC Magnetic Susceptibility Studies. Variable-temperature magnetic susceptibility studies were performed on po-

(22) Dolbecq, A.; Boubekeur, K.; Batail, P.; Canadell, E.; Auban-Senzier, P.; Coulon, C.; Lerstrup, K.; Bechgaard, K. *J. Mater. Chem.* **1995**, *5*, 1707.

wdered samples of complexes **1**·0.08CH_2Cl_2, **4**·0.2CH_2Cl_2, **9**·0.4CH_2Cl_2, and **12**.

Complexes **1** and **4** exhibit behavior expected for high-spin Mn^{III} ($S = 2$) centers exhibiting zero-field splitting (ZFS). To characterize the ZFS parameter D further, magnetization vs field data were collected in the 2.00−4.00 K range in fields of 10.0−50.0 kG. Fits of the data (vide infra for method) gave $S = 2$, $g = 1.96$, and $D = -1.9$ cm^{-1} for **1**, and $S = 2$, $g = 1.93$, and $D = -1.9$ cm^{-1} for **4**.

For complexes **9** and **12**, magnetic susceptibility data were collected in the range 2.00−320 K in an applied field of 10.0 kG (1 T). For complex **9**, the μ_{eff}/μ_B ($\chi_m T$/cm^3 K mol^{-1}) values slowly increase from 16.01 (32.04) at 320 K to a maximum of 24.27 (73.63) at 30.1 K and then decrease to 13.69 (23.43) at 2.00 K (Figure 6). The data for complex **12** were very similar to those for **9**, with values of 16.73 (34.94), 24.60 (75.65), and 13.86 (24.01) at 300, 40.0, and 2.00 K, respectively. The maxima are similar to the 24.99 (78.0) values of a $S = 12$ spin system with $g = 2.00$, suggesting the presence of ferromagnetic coupling in **9** and **12**; the drop at the lowest temperatures is likely due to zero-field splitting, Zeeman effects, and intermolecular interactions.

The Heisenberg exchange Hamiltonian appropriate for a Mn_6 octahedron is given in eq 5,

$$\hat{H} = -2J_{cis}(\hat{S}_1\hat{S}_2 + \hat{S}_1\hat{S}_3 + \hat{S}_1\hat{S}_4 + \hat{S}_1\hat{S}_6 + \hat{S}_2\hat{S}_3 + \hat{S}_2\hat{S}_5 + \hat{S}_2\hat{S}_6 + \hat{S}_3\hat{S}_4 + \hat{S}_3\hat{S}_5 + \hat{S}_4\hat{S}_5 + \hat{S}_4\hat{S}_6 + \hat{S}_5\hat{S}_6) - 2J_{trans}(\hat{S}_1\hat{S}_5 + \hat{S}_2\hat{S}_4 + \hat{S}_3\hat{S}_6) \quad (5)$$

where S_i refers to the spin of metal Mn_i, and J_{cis} and J_{trans} are the pairwise exchange parameters for adjacent and opposite metals of the octahedron, respectively; the Mn labeling scheme of Figures 2 and 3 is employed. This Hamiltonian can be transformed into an equivalent form (eq 6)

$$\hat{H} = -J_{cis}(\hat{S}_T^2 - \hat{S}_A^2 - \hat{S}_B^2 - \hat{S}_C^2) - J_{trans}(\hat{S}_A^2 + \hat{S}_B^2 + \hat{S}_C^2 - \hat{S}_1^2 - \hat{S}_2^2 - \hat{S}_3^2 - \hat{S}_4^2 - \hat{S}_5^2 - \hat{S}_6^2) \quad (6)$$

by use of the Kambe vector coupling method[23a,b] and the substitutions $\hat{S}_A = \hat{S}_1 + \hat{S}_5$, $\hat{S}_B = \hat{S}_2 + \hat{S}_4$, $\hat{S}_C = \hat{S}_3 + \hat{S}_6$ and $\hat{S}_T = \hat{S}_A + \hat{S}_B + \hat{S}_C$ where S_T is the resultant spin of the complete molecule. There are a total of 1751 S_T states for a Mn_6^{III} octahedron ($S_i = 2$) ranging from a single $S_T = 12$ state to 65 different $S_T = 0$ states. From eq 6 can be obtained the energy expression (eq 7) for the

$$E(S_T) = -J_{cis}[S_T(S_T + 1) - S_A(S_A + 1) - S_B(S_B + 1) - S_C(S_C + 1)] - J_{trans}[S_A(S_A + 1) + S_B(S_B + 1) + S_C(S_C + 1)] \quad (7)$$

energies, $E(S_T)$, of each S_T state; constant terms contributing equally to all states have been omitted from eq 7. Using eq 7 and the Van Vleck equation,[23c] a theoretical χ_m vs T equation was derived,[23d] and this was used to fit[23e] the experimental data for **9** and **12**. Only data for the 30.0−300 K range were used, since the model does not incorporate ZFS and other minor effects and therefore cannot reproduce the decrease at lower temperatures. Good fits were obtained for both **9** and **12** with fitting parameters (in the format **9**/**12**) of $J_{cis} = +8.6/+8.5$ cm^{-1}, $J_{trans} = +0.33/-0.31$ cm^{-1}, and $g = 1.96/1.98$, with temperature independent paramagnetism (TIP) held constant at 1200×10^{-6} $cm^3 mol^{-1}$ (solid line in Figure 6). Owing to the small value of J_{trans}, a fit with J_{trans} fixed at zero was also attempted and gave an excellent fit with $J_{cis} = +8.6/+8.5$ cm^{-1} and $g = 1.97/1.98$. The latter fits with $J_{trans} = 0$ are preferred, since they are superimposable to the former fits and involve fewer fitting parameters. Note that J_{trans} is not necessarily zero but it is very small and therefore difficult to quantify reliably.

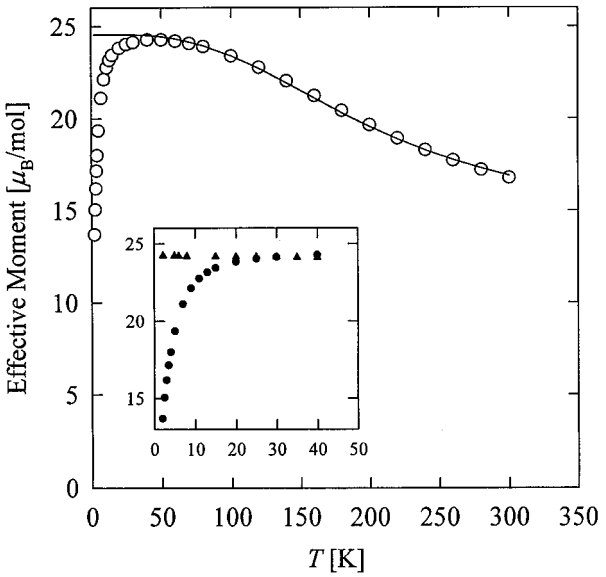

Figure 6. Plot of effective magnetic moment (μ_{eff}) per molecule vs T for $[Mn_6O_4Cl_4(Me_2dbm)_6]$ in a 10.0 kG DC field. The solid line is a fit of the 40.0−300 K data to the appropriate theoretical equation; see the text for the fitting parameters. The inset compares the 2.00−40.0 K DC data (●) with the in-phase (χ_m') AC data (▲).

The fits indicate that the Mn_6 complexes **9** and **12** have $S_T = 12$ ground states. In the notation (S_T, S_A, S_B, S_C), this is the (12, 4, 4, 4) state in which all six Mn^{III} spins are aligned parallel. The first excited state is a triply degenerate set of $S_T = 11$ states comprising the (11, 3, 4, 4), (11, 4, 3, 4), and (11, 4, 4, 3) states at 138 and 136 cm^{-1} above the ground state for **9** and **12**, respectively. The $S = 12$ ground state in these Mn_6 complexes is thus well-isolated from the nearest excited state.

To confirm the $S = 12$ ground states and to obtain values of the ZFS parameter D, magnetization data for **9** and **12** were collected in the 2.00−15.0 K range with applied fields in the 0.500−50.0 kG range. Plots of reduced magnetization ($M/N\mu_B$) vs H/T for **9** are given in Figure 7. The $M/N\mu_B$ values for **9** and **12** saturate at values of 23.02 and 23.62, respectively, with each isofield data set virtually superimposable for each complex. The expected saturation value for an $S = 12$ state with $g = 2.00$ and no ZFS is 24.00, which is close to the observed values. This and the virtually superimposable isofield lines indicate that the ground states of these Mn_6 complexes are characterized by very small values of the ZFS parameter D; this would be consistent with the virtual T_d symmetry of these complexes.

The $M/N\mu_B$ vs H/T data for **9** and **12** were fit by assuming only the ground state is populated in the 2.00−15.0 K range. A spin Hamiltonian was constructed which incorporated isotropic Zeeman splitting and axial ZFS terms ($D\hat{S}_z^2$). This was used to construct the energy matrix for the $S_T = 12$ ground state, which has $(2S + 1)^2 = 625$ matrix elements. An iterative fitting program[2a,23e] which diagonalizes the matrix on each cycle was

(23) (a) Kambe, K. *J. Phys. Soc. Jpn.* **1950**, *5*, 48. (b) Cornia, A.; Gatteschi, D.; Hegetschweiler, K. *Inorg. Chem.* **1994**, *33*, 1559. (c) Carlin, R. L. *Magnetochemistry*, Springer-Verlag: New York, 1986. (d) The equation contains ~1750 terms in each of the numerator and denominator and is thus too long to be presented. See Supporting Information. (e) For the fitting program, see: Schmitt, E. A. Ph.D. Thesis, University of Illinois at Urbana-Champaign, 1995.

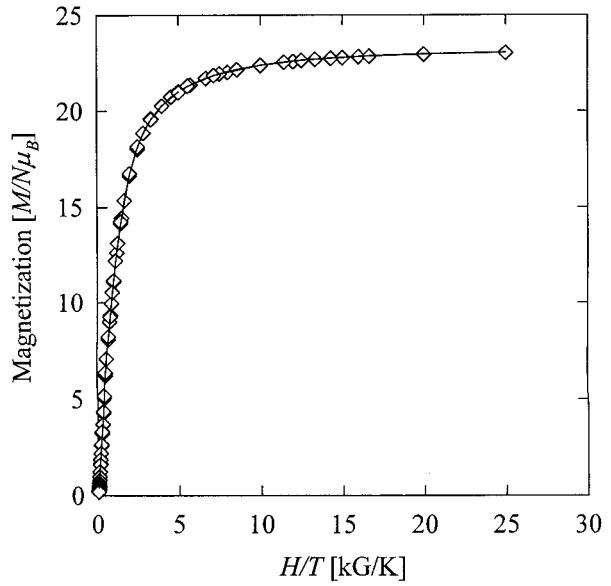

Figure 7. Plot of reduced magnetization ($M/N\mu_B$) vs H/T for $[Mn_6O_4Cl_4(Me_2dbm)_6]$ (**9**) showing data collected in the 2.00−4.00 K ranges and fields up to 50 kG. The solid line is a fit of the data with fitting parameters given in the text.

used to least-squares fit the magnetization data by use of the expression in eq 8,

$$M = \chi_m H = N[\sum(-\delta E/\delta H)\exp(-E/kT)]/\sum\exp(-E/kT)] \quad (8)$$

where $\delta E/\delta H$ is the change in the energy of a given matrix element in response to the magnetic field. The program functioned by stepping through various values g and D for a given spin state in order to find the minimum error between the experimental and calculated susceptibilities. Excellent fits were obtained for **9**/**12** with $S_T = 12$, $g = 1.94/1.98$ and $D = +0.007/-0.011$ cm^{-1}. Given the very small values of D, the latter was fixed at $D = 0$ cm^{-1} and excellent fits were again obtained with $S = 12$ and $g = 1.94/1.98$. The two sets of fits were essentially superimposable, and we thus conclude that $|D| < 0.01$ cm^{-1} for both **9** and **12**. High-frequency EPR experiments are in progress to determine D values more precisely.

The ZFS of the ground state of a polynuclear Mn^{III} complex is largely a consequence of the vectorial addition of the single-ion ZFS tensors. A large Jahn−Teller (JT) distortion is typically seen in an octahedral Mn^{III} ion, in which a unique axis is formed by two noticeably longer Mn−L bond distances. This axis often defines the unique axis of the magnetic structure of the Mn^{III} ion; for example, the g and ZFS tensors will typically have their principal axis along the JT axis. Single-ion ZFS in Mn^{III} ions can be very large; for example, high-frequency EPR experiments have shown that $D = -4.35$ cm^{-1} in $Mn(dbm)_3$.[24] When all JT axes are oriented parallel, the resultant ZFS of a Mn_x^{III} complex will be quite large; for example, in $[Mn_{12}O_{12}(O_2CR)_{16}(H_2O)_4]$ complexes (8 Mn^{III}, 4 Mn^{IV}), the 8 Mn^{III} ions have their JT axes essentially parallel, and the net ZFS in the molecule is fairly large ($D = -0.5$ cm^{-1}).[2,9−11] On the other hand, when the JT axes do not all point in the same direction, the resultant ZFS will be small, as the contributions from the individual sites partially or completely cancel out. In the Mn_6 complexes **9** and **12**, the high symmetry of the molecule ($\sim T_d$) means that the vectorial addition of single ion anisotropies should sum to zero. This is borne out by the experimental observation of $D \approx 0$ for **9** and **12**.

One might ask why the exchange interactions in these Mn_6 complexes are ferromagnetic. Consideration of this question benefits from comparison with the $[Mn_4O_3X(O_2CR)_3(dbm)_3]$ (X = Cl$^-$, Br$^-$ and various others) complexes,[18] which contain a $[Mn_4(\mu_3\text{-}O)_3(\mu_3\text{-}X)]^{6+}$ (3 Mn^{III}, Mn^{IV}) distorted-cubane core of C_{3v} symmetry: the Mn^{III}/Mn^{IV} and Mn^{III}/Mn^{III} interactions are antiferromagnetic ($J_{34} \approx -28$ to -30 cm^{-1}) and ferromagnetic ($J_{33} \approx 8$ cm^{-1}), respectively, with the Mn^{III} pairs bridged by one X$^-$ and one O^{2-} ion, as shown, i.e., the same as in the Mn_6 complexes.

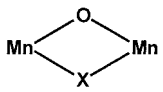

Unfortunately, no *dinuclear* complexes with the $[Mn_2(\mu\text{-}O)(\mu\text{-}X)]$ core are known for comparison, but this unit within both the Mn_4 and Mn_6 clusters leads to ferromagnetic interactions. In both species, the Mn^{III} JT elongation axes intersect at X$^-$ ions: taking this as the local z axis means the singly occupied d_{z^2} orbitals will intersect at the X$^-$ ion. Regardless of whether this σ-superexchange pathway leads to ferro- or antiferromagnetic interactions, the very long Mn−X bonds likely make this a minor contributor to the overall interaction. The dominant superexchange pathways will likely be through the O^{2-} bridges, which also rationalizes why Br-for-Cl substitution has essentially no effect on the J_{33} parameter in the Mn_4 complexes or J_{cis} in **9** vs **12**. A σ pathway through the O^{2-} bridges, which would normally give strong antiferromagnetic coupling at these Mn−O−Mn angles (115−117°) if the metal d_σ orbitals were half-occupied, is nonoperative in these Mn_4 and Mn_6 species because the d_σ ($d_{x^2-y^2}$) orbitals pointing at the O^{2-} ions are empty. The overall coupling between any two Mn^{III} ions thus becomes the balance of several weaker ferromagnetic (J_F) and antiferromagnetic (J_{AF}) contributions, all of which are likely to be of comparable magnitude; the overall J_{obs} should therefore be weak and either side of zero, as was found. Possible contributions include $d^1_\pi - O_\pi - d^1_\pi$ π-overlaps (J_{AF}) and $d^1_{z^2} - O_\sigma - d_{x^2-y^2}$ σ-overlaps (J_F) between empty $d_{x^2-y^2}$ and occupied d_{z^2} (via "doughnuts" in the xy plane). In both the Mn_4 and Mn_6 cases, the J_F contributions win out to give a positive overall J.

AC Magnetic Susceptibility Studies. Since a large ground-state spin value of $S = 12$ had been characterized for the Mn_6 complexes, their AC magnetic susceptibilities were investigated to check for the presence of slow magnetic relaxation. Other molecules with large spin ground states, such as the $[Mn_{12}O_{12}(O_2CR)_{16}(H_2O)_4]$ complex with $S = 10$, have been shown to act as superparamagnets at near liquid He temperatures, as shown by the presence of an out-of-phase AC susceptibility signal (χ_m'') for fields oscillating at frequencies ≤1500 Hz.[2,6] A superparamagnet is a subtype of a magnet in which the number of interacting spin carriers is too small to form more than one domain, and thus it is a single-domain magnetic particle consisting of up to several thousand interacting metal ions/spin carriers yielding a large net spin. A superparamagnet exhibits slow magnetic relaxation (reorientation of its magnetization vector), resulting in an out-of-phase signal when examined by AC susceptibility. The Mn_{12} complex is thus one of the smallest superparamagnets, consisting of only 12 interacting spin carriers and yielding a net spin of $S = 10$; similarly certain Mn_4,[8] V_4,[25] Fe_8,[12] and Mn_{11}[5c,11b] clusters are other examples of molecular superparamagnets which have been termed single-molecule

(24) Barra, A.-L.; Gatteschi, D.; Sessoli, R.; Abbati, G. L.; Cornia, A.; Fabretti, A. C.; Uytterhoeven, M. G. *Angew. Chem., Int. Ed. Engl.* **1997**, *36*, 2329.

magnets[8a] to reflect their unusual properties. The slow relaxation is caused by magnetic anisotropy resulting from a combination of a large ground-state spin (S) value and a large and negative zero-field splitting (ZFS) parameter D. This results in a potential energy barrier to relaxation of $S^2|D|$, or $\sim$50 cm^{-1} for $S = 10$ and $D \approx -0.5$ cm^{-1} as found in the Mn_{12} complexes.[2,6,26] The Mn_6 complexes **9** and **12** have a large spin of $S = 12$ but virtually no magnetic anisotropy as reflected in D values of $\leq$0.01 cm^{-1}, corresponding to an energy barrier for magnetization reversal of $\leq$1.44 cm^{-1}; the latter is much too small to cause slow magnetic relaxation and the appearance of χ_m'' signals in AC susceptibility studies. Nevertheless, it was hoped that, as for the V_4 complexes $[V_4O_2(O_2CR)_7(L-L)_2]^z$ (L−L = bpy, $z = +1$; pic, $z = -1$),[25] application of a DC field would cause the rate of magnetization reversal to decrease sufficiently to permit observation of χ_m'' signals. The AC susceptibilities of complexes **9** and **12** were collected initially in zero DC field over the 2.00 to 40.0 K temperature range in a 1 G field oscillating at 997 Hz. Both complexes gave essentially the same behavior, and only the results for **9** will thus be detailed. The insert to Figure 6 contains the AC susceptibility data for **9**, in which the in-phase susceptibility (χ_m') is plotted as μ_{eff}/μ_B and compared with the DC effective magnetic moment in a 10.0 kG DC field. The out-of-phase signal (χ_m'') was zero at all temperatures down to 2.00 K. The AC μ_{eff} value was constant at 24.2 μ_B in the 2.00−40.0 K range in contrast to the DC μ_{eff} value which decreased with decreasing temperature. The expected spin-only ($g = 2.0$) μ_{eff} value for a $S = 12$ state is 25.0 μ_B, very close to the observed AC value. As no χ_m'' signal was observed, the difference between the AC and DC data sets arises not from relaxation effects but from the effects of the 10.0 kG DC field.

An interesting question arises, however. What is the AC susceptibility response in the presence of a modest DC field? The AC susceptibilities of **9** and **12** were measured over a wide range of applied DC fields in the 0.500−7.00 kG range between 1.71 and 10.0 K. Out-of-phase signals were observed in all isofield data sets, indicating slow magnetic relaxation; one set of experimental data for complex **9** at 2.00 K is shown in Figure 8. The data are presented in the form of normalized Cole−Cole (or Argand) plots, in which the out-of-phase (χ_m'') and in-phase (χ_m') susceptibilities obtained at a given AC frequency are plotted as a single point, with χ_m'' plotted as a function of χ_m'. For each AC frequency used (0.74−1512 Hz), a different datum point is plotted. At 2.00 K, each Argand plot is clearly the sum of two overlapping arcs that are only partially defined by the experimental data. The Argand plots at 4.50 K (not shown) are also clearly composed of two arcs. For a single relaxation process, an Argand diagram has the form of a single arc in which the point at the arc's maximum indicates the frequency for which the condition $\omega\tau = 1$ is met,[27] where ω is the angular frequency of the AC field ($\omega = 2\pi\nu$) and τ is the characteristic lifetime for that relaxation process. When the relaxation process is characterized by a single lifetime, the arc will form a semicircle that has its origin on the χ_m' axis. The relaxation process more typically will be characterized by a distribution of lifetimes, and the semicircle has its origin below the χ_m' axis. In such instances, as for Mn_6, it is more appropriate to speak of an average τ for the relaxation process. What is immediately apparent is that there are two relaxation processes for Mn_6 in the presence of an applied DC field, each of which has an average relaxation rate constant ($k = 1/\tau$) near that of the oscillating AC field (0.74−1512 Hz).

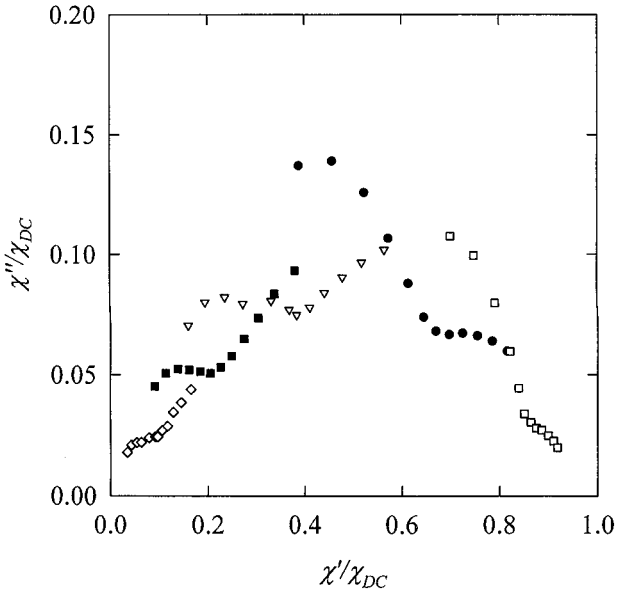

Figure 8. Argand plot for $[Mn_6O_4Cl_4(Me_2dbm)_6]$ (**9**) at 2.00 K at AC frequencies in the 0.74−1512 Hz range and applied DC fields of 500 (□), 1000 (●), 2000 (▽), 3000 (■) and 6000 (◇) G.

There are three basic relaxation mechanisms: the direct, Raman, and Orbach processes.[27b,28] Each mechanism involves the absorption of lattice vibrational (phonon) energy to induce changes in the populations of different energy levels, with different dependencies upon field (H) and temperature (T). In the simplest picture of magnetic relaxation, a molecule converts between two states ($|a\rangle$ and $|b\rangle$) that differ in energy by Δ. The direct process involves the absorption of one phonon whose energy matches Δ, which results in a transition between the levels $|a\rangle$ and $|b\rangle$. The Raman process involves an excited virtual energy level ($|c\rangle$) and operates by the spontaneous absorption and emission of two phonons whose energy difference matches Δ. The Orbach process is similar to the Raman process, but the excited energy level $|c\rangle$ is in thermal equilibrium with the levels $|a\rangle$ and $|b\rangle$. Direct processes often dominate relaxation mechanisms at low temperatures but tend to have a limiting dependence upon H and T ($k \propto H^2T$).[23c] Raman mechanisms have a large dependence upon temperature ($k \propto T^{7-9}$),[23c] and therefore are less likely to dominate relaxation mechanisms at the low temperatures studied here. The most likely origin of the two observed relaxation processes is a thermally activated (Orbach) relaxation process.

Conclusions

Convenient procedures have been developed to the five-coordinate complexes $[MnX(R_2dbm)_2]$ (X = Cl, Br; R = H, Me, Et), containing high-spin Mn^{III} in square-pyramidal coordination geometry. The R = Me and Et derivatives have proved to be excellent starting points for the synthesis of a new class of Mn cluster of formulation $[Mn_6O_4X_4(R_2dbm)_6]$ (X = Cl, Br). These clusters contain a Mn_6^{III} octahedron with a combination

(25) Castro, S. L.; Sun, Z.; Grant, C. M.; Bollinger, J. C.; Hendrickson, D. N.; Christou, G. *J. Am. Chem. Soc.* **1998**, *120*, 2365.

(26) (a) Aubin, S. M. J.; Spagna, S.; Eppley, H. J.; Sager, R. E.; Christou, G.; Hendrickson, D. N. *Chem. Commun.* **1998**, 803. (b) Aubin, S. M. J.; Sun, Z.; Gruzei, I. A.; Rheingold, A. L.; Christou, G.; Hendrickson, D. N. *Chem. Commun.* **1997**, 2239.

(27) (a) van Duyneveldt, A. J., Lakeshore Cryotonocs, Inc., application note for model 7000 AC susceptometer, Lakeshore Cryotonics, Westerville, Ohio. (b) van Duyneveldt, A. J. In *Magnetic Molecular Materials*; Gatteschi, D., Kahn, O., Miller, J., Palacio, F., Eds., Kluwer Academic Publishers: London, 1991.

(28) Abragam, A.; Bleaney, B. *Electron Paramagnetic Resonance of Transition Ions*; Dover Press: Mineola, New York, 1986.

of μ_3-O^{2-} and μ_3-X^- bridges on the faces. In addition to its structural aesthetics, this cluster type has been found to be a rare example of a completely ferromagnetically coupled multinuclear species, and as a result, these Mn_6 species have $S = 12$ ground states, the joint-highest yet observed for Mn and one of the highest for any metal. Three other $S = 12$ Mn clusters are also known, and two of these also happen to be hexanuclear,[4c,h] the third being decanuclear.[4d] The present Mn_6 clusters thus join a still small but continually growing family of high-spin ($S \geq 4$) clusters, the majority of which are in Mn chemistry. Unfortunately, however, the present Mn_6 clusters are not new additions to the small group of species exhibiting the new magnetic phenomenon of single-molecule magnetism. This can be explained by their high (T_d) symmetry, which averages out to zero the magnetic anisotropy resulting from single-ion zero-field splitting effects in Jahn−Teller distorted Mn^{III}. Consequently, although one requirement for a single-molecule magnet (SMM) is fulfilled, i.e., a high-spin ground state, the second requirement of a large, negative ZFS parameter D is not fulfilled. The Mn_6 species have D values ≤ 0.01 cm^{-1}, too small to yield a sufficiently large barrier $S^2|D|$ to magnetization reversal. As a result, they do not exhibit the slow magnetic relaxation that would yield, for example, magnetization hysteresis curves. Nevertheless, the Mn_6 complexes represent an important step forward in the overall objective of developing synthetic procedures to high-spin clusters and understanding both (i) the factors that yield large ground-state spin values and reasonably large magnetic anisotropies and (ii) the behavior of such species in DC and/or AC magnetic fields. This understanding is important to the future progress of the new field of single-molecule magnetism.

Acknowledgment. This work was supported by the National Science Foundation (D.N.H. and G.C.). The AC measurements were performed with a MPMS2 SQUID magnetometer provided by the Center for Interface and Material Science, funded by the W. M. Keck Foundation.

Supporting Information Available: Tables of crystal data, structure solution and refinement, atomic coordinates, anisotropic thermal parameters, and bond distances and angles for complexes **1**, **4**, **9** and **10** and unit cell packing diagrams for **1** and **4**; listing of the S_T states for an Mn_6^{III} octahedron (PDF) and a crystallographic file in CIF format. This material is available free of charge via the Internet at http://pubs.acs.org.

JA983446C